Eur. Phys. J. Special Topics **223**, 1755–1769 (2014)

DOI: 10.1140/epjst/e2014-02224-9

THE EUROPEAN PHYSICAL JOURNAL SPECIAL TOPICS

Regular Article

Adhesion of giant unilamellar vesicles on double-end grafted DNA carpets

Y. Sun, C.M. Marques, and A.P. Schroder[a]

Institut Charles Sadron, Université de Strasbourg, CNRS UPR22, 67034 Strasbourg, France

Received 30 June 2014 / Received in final form 21 July 2014
Published online 22 September 2014

Abstract. We have recently shown that the bio-mimetic adhesion of Giant Unilamellar Vesicles on carpets of lambda-phage DNAs, grafted by one end to the substrate, leads to DNA scraping and stapling. As the lipid adhesion patch is built, outward forces stretch the DNA, while adhesion patch formation staples the chains into frozen conformations, trapped between the GUV membrane and the substrate. Analysis of the scraped and stapled DNA conformations provides a wealth of information about the membrane/polymer interactions at play during the formation of a bio-adhesive contact zone. In this paper we report new phenomena revealed by scraping and stapling phenomena associated with the bio-mimetic adhesion of Giant Unilamellar Vesicles on carpets of lambda-phage DNAs that were grafted to the substrate by both ends. In particular, the peculiar shapes of stapled DNA observed in this case, suggest that the membrane exerces not only outward radial forces during patch formation, but is is also able to confine the DNA molecules in the orthoradial direction.

1 Introduction

Phospholipid membranes are self assembled bilayers that host, in the cell plasma membrane and in the cell organelles, a variety of bio-macromolecules for structure and function. Bio-mimetic constructs of the cell membranes can be self-assembled from a limited number of phospholipids and other molecules, in order to study cell adhesion and other fundamental cell phenomena in a simple physical and chemical environment. We have recently developed [1] a model system for understanding the different forces at play during the formation of a bio-adhesive contact that typically implies a lipid membrane with its adhesive binders, a complementary functional substrate and the different macromolecular species that decorate both the membrane and the substrate.

Our experimental model consists in a bio-adhesive phospholipid vesicle that is brought into contact with a carpeted surface of end-grafted lambda-phage DNAs. During contact, the spreading front of the adhesive patch propagates outwards from a nucleation center, acting as a scraper that strongly stretches the DNA chains. Moreover, the multiple adhesion bonds created during vesicle spreading effectively staple

[a] e-mail: andre.schroder@ics-cnrs.unistra.fr

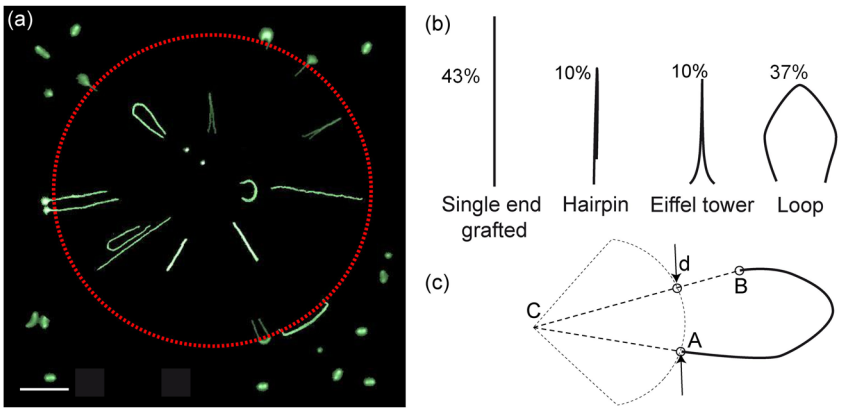

Fig. 1. (a) Typical landscape in the adhesion region of a GUV. The border of the adhesion patch is given by the dotted circle and can be clearly identified in a Reflexion Interference Contrast (RICM) image (not shown). Bar is 10 μm; (b) the four typical configurations observed, and their relative fraction; (c) the projected distance d of the end-to-end distance of the grafted DNA on the direction perpendicular to the adhesion radial direction: A and B are the DNA grafting ends, C is the center of the vesicle adhesion patch.

the stretched chains in the gap between the membrane and the substrate, creating a tunnel-like channel for the macromolecules. The trapped chain configuration starts thus at its fixed, end-grafted point on the substrate, meandering through a forest of short polymer bonds that connect the phospholipid membrane above the chain to the protein bed below it, eventually exiting the adhesive gap to adopt a coil-like configuration in the corner between the vertical vesicle wall and the protein surface.

This experimental geometry provides not only key information about chain conformations in the adhesive patch but also shows that forces induced on the chain by the formation of the adhesive contact are a combination of solvent mediated shear stresses and direct membrane interactions [1]. However, lack of force calibration has precluded in previous experiments a quantitative analysis of the different forces involved. In this paper, by combining experiments on double-end grafted DNA chains with a numerical simulation of the spreading process we unveil the surprising features of the formation of DNA stretched loops under the forces generated by the bilayer adhesive contact.

2 Results and discussions

2.1 Adhesion landscape

A typical DNA landscape under an adhered vesicle is given by Fig. 1a, as observed with fluorescence microscopy. The image is an average over *circa* one hundred images, taken at the end of the adhesion process, when both the membrane and the DNAs are in a long term, stable geometrical configuration. The dotted circle (red online) in Fig. 1a sketches the limit of the adhesion patch, that cannot be visualized in the fluorescence observation mode but can be seen in RICM picture. The surface end-grafted DNA molecules are seen as bright objects. Inside the adhesion patch region, the DNAs appear significantly elongated, as expected from stretching and confinement by vesicle spreading [1]. Making statistics over circa eight hundred DNAs taken in the adhesion patch region, we were able to classify the end-grafted molecules into four

classes: single-end grafted (43%), and double-end grafted (57%), that can further be classified into "hairpins" (10%), "Eiffel towers" (10%), and "loops" (37%) (Fig. 1b). The proportion of single end-grafted DNAs quantifies chains with single biotinylated ends. Outside the adhesion patch the grafted DNAs appear either as circular dots of roughly one-micrometer size, or as slightly elongated objects with a mask-like shape. The former correspond to single-end grafted DNAs and the latter to double-end grafted chains.

Single-end grafted chains confirm our previous observation that the stretching force exerted by the advancing membrane front during the adhesion is radially oriented [1]. We also measured the relative quantities of each of the three kinds of DNA configurations for double-end grafted chains (*i.e.* hairpins, Eiffel towers and loops) as a function of the ligand density in the adhering GUVs. Surprisingly, these relative fractions are roughly constant with respect to the ligand density (not shown). Thus the relative formation of these different configurations is not influenced, within the range of adhesion-bond density explored here (0.2–4 mole%), by the kinetics of vesicle spreading.

The analysis of the double end-grafted chains revealed that hairpins correspond to DNA chains with grafted ends almost perfectly aligned with the radial direction. The distributions of "Eiffel towers" and "loops" (not shown) are well described as a function of the projected orthoradial distance d between the two grafted ends of the chain (Fig. 1c). We measured the following values for the projected distance d: $d_{Eiffel} = 1.0 \pm 0.5$ μm for "Eiffel towers", and $d_{loop} = 1.6 \pm 0.8$ μm for "loops". We focus in this paper on the analysis of the loop-shaped DNAs.

2.2 Loops characteristics

This study concerns the analysis of final, time averaged images, obtained once the adhesion process has stopped. Average images have a much better signal/noise ratio than real time images, enabling improved image analysis. We analyzed between ten and twenty DNA loops for each of the following values of the ligand density ρ in the membrane, expressed as the biotin/DOPC molar ratio: 1/25, 1/50, 1/100, 1/200, and 1/500.

An example of two stretched DNAs trapped under the membrane is given in Fig. 2a. We used a homemade program (see Experimental section) to squeletonize each DNA image, and to measure its intensity profile, as shown in Fig. 2b. Here the fluorescence intensity is represented as a function of the cumulated perimeter, *i.e.* the curvilinear distance along the digitized molecule, starting from one reference end. Figure 2b is typical of what we measured for all the DNAs: the fluorescence intensity appears constant along the stretched, confined molecule, with a noise of circa ±10%. We therefore assume that the monomer density is constant along a confined DNA loop, corresponding to an homogeneous stretching degree of the double-end-grafted molecule.

The average stretching degree of a stabilized, confined loop is $\alpha_{conf}^{final} = l_{app}/L_0$, where l_{app} is the apparent perimeter of the squeletonized loop (*i.e.* the final value of the cumulated perimeter in Fig. 2b), and L_0 is the DNA contour length, taken as $L_0 = 22.0$ μm for $\lambda-$phage DNA with intercalated Yoyo [2]. For each value of the biotin/DOPC fraction in the membrane ρ, the average value $< \alpha_{conf}^{final} >$ taken over ten to twenty DNA loops is given in Fig. 3 as a function of $1/\rho$. $< \alpha_{conf}^{final} >$ is in the range [0.80..0.95], a narrow range indicating that the DNA loops assume strongly stretched configurations. As allready reported elsewhere [1] for similar biotin contents, the membrane front spreading velocity lies in the range 1..10 μms^{-1}, that

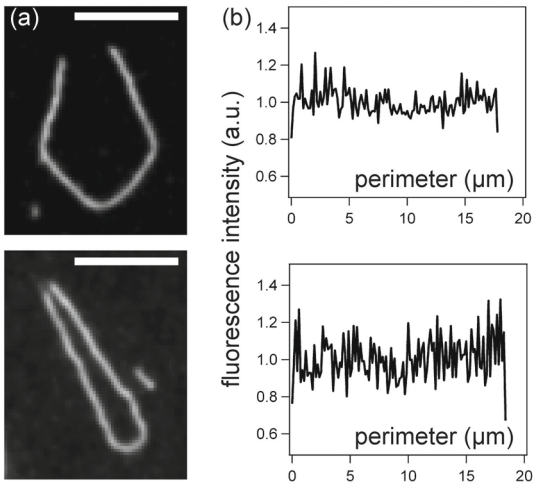

Fig. 2. (a) Two typical DNAs stretched and confined in the membrane-substrate gap of an adhered DOPC GUV. The constrast has been enhanced. Bar is 5 μm; (b) intensity profile along the molecule, measured as explained in the Experimental Section.

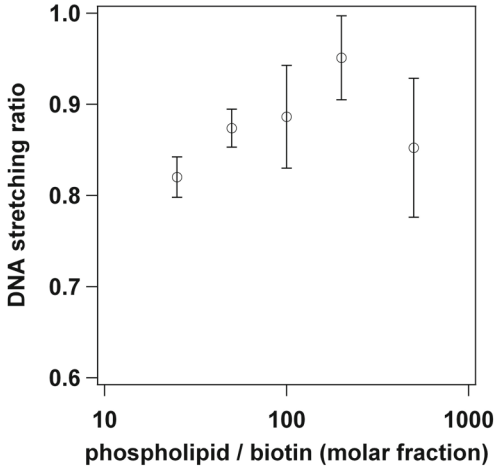

Fig. 3. Averaged value $< \alpha_{conf}^{final} >$ over typically ten to twenty DNAs of the loop average stretching ratio $\alpha_{conf}^{final} = l_{app}/L_0$, as a function of $1/\rho$.

corresponds to shear rates $\dot{\gamma}$ in the range $\sim 10^2$ to $10^3\,\mathrm{s}^{-1}$ for the end-grafted DNAs (see the complete discussion in the Experimental section). Thus the caracteristic time of shearing in the membrane substrate gap is higher than the slower relaxation mode of λ-phage DNA, that has been measured to be of the order of 400 ms [3]. Last but not least, the numerous biotin ligands populating the membrane surface rapidly bind to the surface during spreading, building a tunnel that confines the elongated chain. This explains the measured high values for DNA stretching $< \alpha_{conf}^{final} >$ in the present configuration.

The squeletons of the DNAs of Fig. 2a are shown in Fig. 4a, with a rotation that brings each loop symmetry main axis parallel to the vertical y-axis. We define θ as the local orientation of a DNA squeletton, with respect to the y-axis, averaged over four consecutive points (Fig. 4a). Figure 4b represents θ as a function of the cumulated

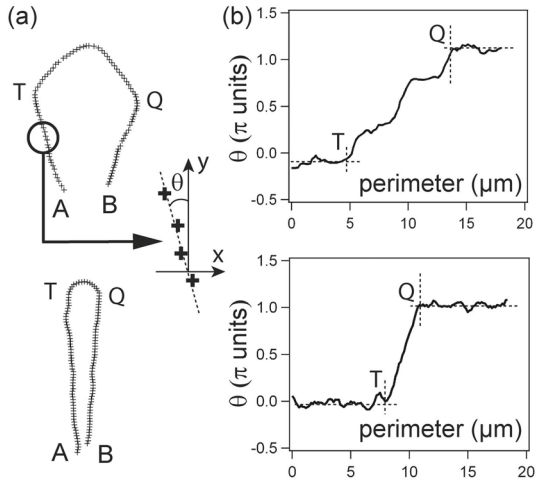

Fig. 4. (a) Digital profiles of the two DNAs shown in Fig. 2. The profiles have been rotated around the adhesion patch center, so to align the loop symmetry axis parallel to the y-axis. At any place of the contour, the local angle θ with respect to the y-axis has been calculated as the average orientation over four consecutive points. (b) θ versus cumulated perimeter, starting from the left end of the rotated profile, for the two DNAs.

perimeter. As highlighted by the figure, for most of the DNA loops studied, the curve of θ vs. perimeter can be divided in three, well defined regions, *i.e.* two ending plateaus and a transition region in-between. Let T and Q be the transition points between the ending plateaus and the medium region of the curve: reporting these points on the corresponding loop unveils two straight segments AT and BQ, where A and B are the two grafting points (see Fig. 4a). We observed that, for almost all the DNA loops, these two ending segments converge nicely on the adhesion patch center, with a precision of less than one micrometer. Thus, this characteristic loop shape seems to indicate that during membrane spreading, from when the membrane front reaches the grafting ends, up to when it reaches the two transition points T and Q (Figs. 4a and b), the spreading imposes a purely radial stretching to the DNA, similarly to what has been reported with single-end grafted DNAs [1], *i.e.* as if the two DNA grafted ends were independent single-end grafted molecules. Note that the medium "capping" region, bounded by the points T and Q, appears to be "V"-like shaped for about 80% of the observed loops, and approximately hemicap-like, as shown in Fig. 2a in the other cases.

The generic trend observed above is sketched in Figs. 5a and 5b. In Fig. 5a the membrane did not reach yet the so-called "transition points" T and Q, and the two DNA embedded "arms" display a radial orientation; each "arm" is in the one-grafted-like stretching regime. In Fig. 5b the loop is in the "cap" formation stage. From the experimental point of view, catching such events is possible but difficult. First, the adhesion of a vesicle takes place in a few seconds only, depending on the biotin/DOPC fraction in the membrane, that requires fast acquisition imaging of the fluorescent DNAs, *i.e.* in low light intensity conditions. Secondly, since predicting where an adhesion will take place is difficult, the sample has to be observed under 'blind' conditions, pending for an adhesion event, a period over which the fluorescent molecule YOYO bleaches, that decreases the signal/noise ratio in the image. Figures 5c and 5d are typical real time images that confirm the sketches of Figs. 5a and 5b. In Fig. 5c, the membrane front is represented by the dotted arc. The arrow shows a DNA loop that is incompletely formed, typical of what is sketched in Fig. 5a.

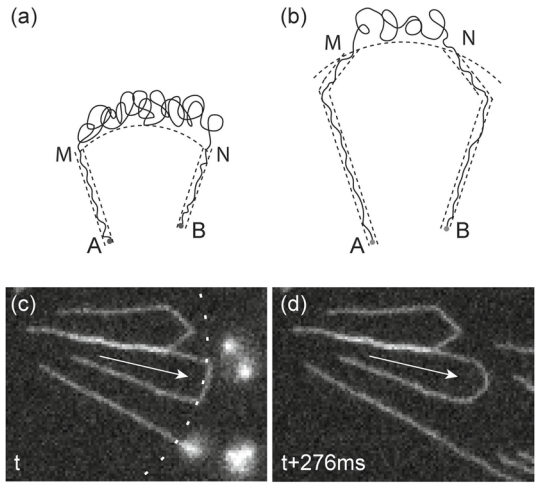

Fig. 5. (a) Sketch of the double-end grafted DNA being pushed away by the membrane advancing front, during the "radial stretching" stage. The dotted arc corresponds to the membrane position and the dotted straight lines sketch the membrane tunnels that confine the two DNA ending segments. (b) Sketch of the molecule at a later moment, when the molecule is in the "cap formation" stage. Dotted arc and straight lines sketch, as for (a), membrane position and confining tunnels. (c) and (d) Fluorescence images of a DNA carpet during membrane adhesion. In (c) the membrane front position is sketched by the dotted arc. In (d) the membrane front is out of the field. The arrow represents the DNA of interest, as well as the direction of membrane spreading. The two pictures are separated by 0.28 s, typical of our maximum acquisition rate of *circa* 3 im./s.

Another loop is totally embedded below the membrane, a single-end grafted DNA is still being stretched, and a few DNAs haven't still been pushed away and confined by the advancing front. In Fig. 5d, the membrane front is already out of the image field, resulting in this case into the formation of a new embedded loop (arrow). Note that, due to the maximum acquisition rates available to us in these low light conditions, we could not catch an intermediate situation corresponding to the sketch of Fig. 5b. Figures 5c and 5d exemplify the lower signal/noise ratio of real time images as compared to average ones (see Fig. 2a).

2.3 "At equilibrium" confinement

Exploring further the possibility of a threshold between an initial radial stretching regime and a second, cap forming one, we analyse each DNA loop as the result of a dynamic process during which the double-end grafted molecule is stretched and pushed away by the spreading front while a membrane tunnel is forming backward above the confined part of the molecule, stabilizing definitely this stretched state. More precisely, we assume that $\alpha_{conf}(t)$, the stretching degree of the growing, embedded part of the DNA (*i.e.* segments AM and BN in Fig. 5) remains constant with time t all along the stretching process, taking its final, equilibrium value $\alpha_{conf}(t) = \alpha_{conf}^{final}$ from the early moments of the DNA confinement in the membrane-substrate gap. Though this assumption can not be stricktly checked without analysing real time images, it is however sustained by the fact that the embedded, final loops exhibit a high, close to the unity stretching degree $0.8 < \alpha_{conf}^{final} < 0.95$ (Fig. 3). Then for any DNA loop considered at time t_{trans}, defined as the time when the membrane reaches the

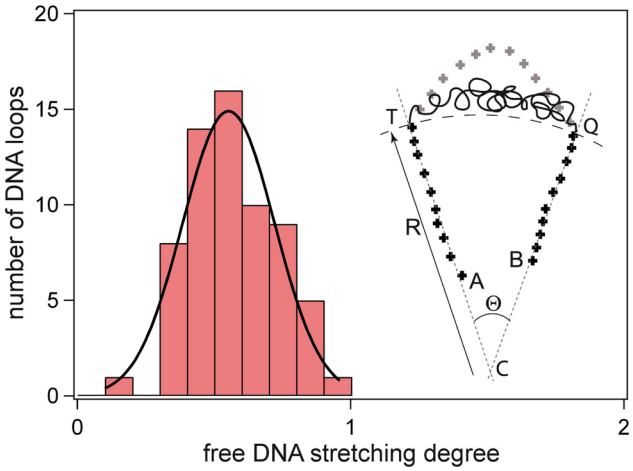

Fig. 6. Sketch of a DNA loop at the precise moment t_{trans} of the transition between the radial stretching regime and the "cap" forming stage. The membrane has just reached points T and Q (dotted arc). Crosses represent the digitized contour of the final, immobilized loop, as obtained from image analysis. AT and BQ are stretched segments of the molecule, while the rest of the DNA remains in a coil conformation in front of the spreading front. R is the distance from the adhesion patch center C and the membrane, and Θ is the angle between the two stretched ends of the DNA. The histogram gives the distribution of $\alpha_{free}(t_{trans})$ as measured over circa 80 loops.

transition points T and Q (Fig. 4), the total contour length of DNA embedded under the membrane is simply $L_{conf}(t_{trans}) = (\|AT\| + \|BQ\|)/\alpha_{conf}^{final}$. Consequently, the contour length of the still fluctuating, partly stretched part of the molecule, located in front of the membrane front at time t_{trans} is $L_{free}(t_{trans}) = L_0 - L_{conf}(t_{trans})$. Finally, the stretching degree at t_{trans} of this fluctuating part of the molecule is $\alpha_{free}(t_{trans}) = R\Theta/L_{free}(t_{trans})$, and R and Θ are simple geometrical parameters defined in Fig. 6. The figure sketches the DNA shape at time t_{trans}, and summarizes the measurement of $\alpha_{free}(t_{trans})$ for all the DNA loops studied here, whatever the biotin density ρ: $\alpha_{free}(t_{trans})$ shows a gaussian distribution around the average value $\alpha_{free}(t_{trans}) = 0.55 \pm 0.09$. Please note that again, we do not observe any effect of the membrane spreading velocity on this quantity.

Thus, indentifying on each DNA loop the transition points T and Q and assuming that the confinement of the DNA is performed at equilibrium during the overall stretching process enables to measure an average, "threshold" value of the internal, stretching degree of the coil-shaped part of DNA that is pushed away by the advancing membrane front, at the apparent moment of the transition between a first radial stretching regime and a second cap forming stage. In other words, we propose here a two step process for the scenario of the DNA loop formation during membrane spreading: in a first step the membrane embeds the DNA under two radially oriented tunnels, consuming DNA length and pushing the rest of the molecule on its front in a partly free, fluctuating, incrisingly stretched configuration, up to a transition point corresponding to a particular value of the internal stretching degree along this free part of the DNA molecule, *i.e.* $\alpha_{free}(t_{trans})$. From then on, the cap formation is initiated, corresponding to the second step of the loop formation. Considering that the DNA fraction that is pushed away by the membrane obeys usual laws for a stretched DNA chain at any time during the membrane spreading, enables to calculate the corresponding internal force at the transition, using Eq. (3): $f_{free}(t_{trans}) = 1.53\ k_BT/l_P$.

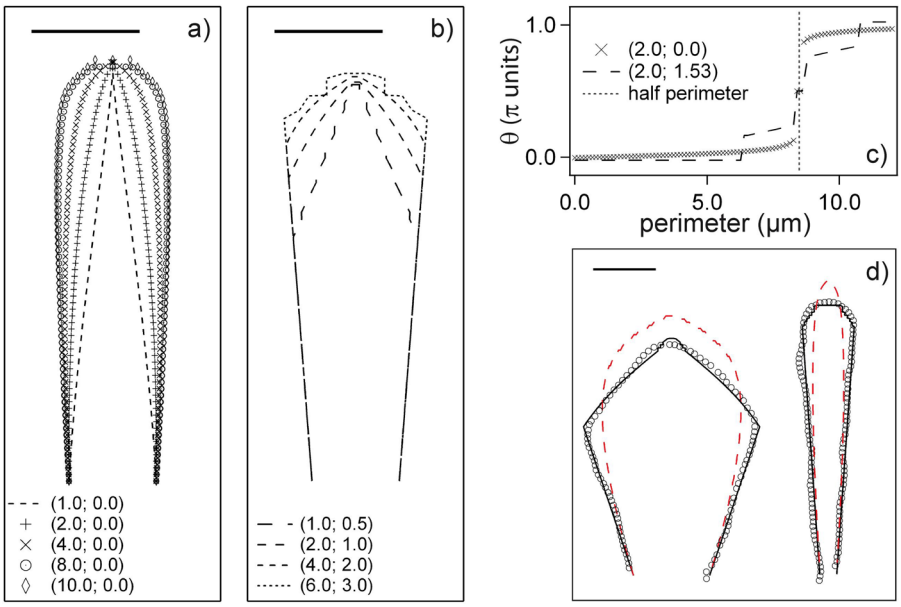

Fig. 7. a) Simulated DNAs obtained for various values of the membrane pushing force, without the presence of the threshold force ($\|\mathbf{F}_{ext}\|$, $f_{thres} = 0$); b) simulated DNAs obtained for various couples ($\|\mathbf{F}_{ext}\|$, f_{thres}); c) local orientation θ (as defined in Fig. 4) along two simulated DNAs; d) same DNAs as in Fig. 4, and the best fits obtained from the simulation. With (——) and without (- - -) a threshold force. All forces are in k_BT/l_p units. Bars are 2.5 μm.

2.4 Loop formation simulation

In order to further interpret the observed loop shapes, and eventually confirm the existence of a two step scenario for the loop formation, we developped a numerical simulation method described in the experimental section. The main results of the simulations are given in Fig. 7. We consider a DNA with its two grafted ends separated by 1.6 μm, at a distance from the adhesion patch center of 11.4 μm, two quantities corresponding to their respective average values over all the observed samples. In Fig. 7a, the simulation runs by achieving at each step the force balance $\|\mathbf{F}_{ext} + \mathbf{F}_{free}\| = \|\mathbf{F}_{conf}\|$, as described in the experimental section. This corresponds to the "classical image" of what is expected to be the interaction between a fluid advancing wall and a coil macromolecule that it pushes away on its front. The various DNAs in Fig. 7a are obtained for values of $\|\mathbf{F}_{ext}\|$ taken in the range [1..10] in k_BT/l_P units. For $\|\mathbf{F}_{ext}\| = 1.0\ k_BT/l_P$ the shape of the DNA loop is clearly different than any observed loop, with an overall "V-shape". For higher values of $\|\mathbf{F}_{ext}\|$ the DNA loop appears shaped as a warhead, but we notice that there is no clear transition between an initial, radial stretching regime and a second, cap forming stage. For the two highest values of $\|\mathbf{F}_{ext}\|$, the DNA exhibits a plateau at the top of the cap. Please note that for $\|\mathbf{F}_{ext}\|$ taken in the range [1..10] k_BT/l_P, the average final stretching of the DNA α_{conf}^{final} is in the range [0.84..0.92], *i.e.* in the range of the measured values (Fig. 3).

As detailed in the experimental section, a lateral threshold force $\mathbf{F}_{thres}$ can be added to the above force balance so that $\mathbf{F}_{thres} = -\mathbf{F}_{free}$ as long as $\|\mathbf{F}_{free}\|$ remains smaller than a given value f_{thres}, and $\mathbf{F}_{thres} = \mathbf{0}$ if $\|\mathbf{F}_{free}\| > f_{thres}$. In other words, the DNA strands undergoing stretching at the adhesion front are trapped in a radial

confinement potential from where they only escape when the orthoradial force exceeds a certain threshold value. Figure 7b shows DNA simulated profiles for various couples of the forces ($\|\mathbf{F}_{ext}\|$, f_{thres}). Here one clearly gets qualitatively similar features than the experimental ones, *i.e.* two straigth, radially stretched segments closed by a "V" – like shaped cap. Please note that as for Fig. 7a, the DNAs exhibit a plateau at the top of the ending cap for the highest values of $\|\mathbf{F}_{ext}\|$.

Figure 7c highlights equally the benefit of considering a threshold force in the force balance. The figure compares the evolution of the local orientation θ (as defined in Fig. 4) vs. the cumulative perimeter in the absence and in the presence of the threshold force into the force balance. Without the threshold force, θ grows gently and continuously with the perimeter, up to a point where it abruptly passes accross $\pi/2$, with a "say" width of transition extending over less than 1 μm. On the contrary, when a threshold force is taken into account in the force balance (here $f_{thres} = 1.53\, k_B T/l_p$), we observe a well defined ending plateau, followed by the cap region extending over typically 5 μm, that corresponds to what we observe experimentally on the average (see Fig. 4b).

We fitted each of our eighty DNA loop profiles using our simulation method, in absence and in presence of a threshold force. Without the threshold force, we considered as the best fit the profile obtained for a value of $\mathbf{F}_{ext}$ leading to the measured average stretching degree of the loop α_{conf}^{final}. Fitting the loops with a threshold force was obtained with a different approach: we first extracted the value of $\alpha_{free}(t_{trans})$ from the analysis of the digitized loop, and then, looked for the best fit by varying the amplitude of $\mathbf{F}_{ext}$. The procedure showed that the loops were better fitted with the threshold force $f_{thres} = f_{free}(t_{trans})$ in the force balance, as exemplified in Fig. 7d for the two DNA loops of Fig. 4a.

However, in the case of the loops with the highest stretching degree, *i.e.* close to one, for which high values of $\|\mathbf{F}_{ext}\| > 10\ k_B T$ had to be considered in the fitting procedure, taking into account the threshold force brought poor advantage to the fitting procedure.

3 Experimental

3.1 Microscopy

All samples were observed using brigth field, fluorescence and Reflexion Interference Contrast Microscopy (RICM) [4], under a TE200 Nikon microscope, equiped with a 100X oil immersion objective (RC-type objective, Leica). RICM enabled to visualize the adhesion patches and to measure the average distance between the membrane and the substrate; we measured $h = 10 \pm 3$ nm with no noticeable effect of the biotin content, a value that is in agreement with other similar measurements [5].

3.2 Streptavidin-coated substrates

We followed a protocol allready described elsewhere [1]. Glass coverslips were first cleaned with Piranha (70% concentrated sulphuric acid H_2SO_4 and 30% hydrogen peroxide H_2O_2 (30%)), and then amino-functionalized by immersion in a mixture of 98% ethanol and 2% 3-aminopropyltriethoxysilane (APTES, Sigma-Aldrich). Followed a 30 minutes exposure of the slide to a 8% solution droplet of glutaraldehyde (Polysciences) and subsequent rinsing with saline phosphate buffer (PBS). Streptavidin (Molecular Probes) was dissolved in PBS at 4 mg ml^{-1}; a droplet of this solution was then deposited on the slide and rinsed after one hour with Tris-borate-EDTA buffer (TBE).

3.3 Giant unilamellar vesicles preparation

Giant Unilamellar Vesicles (GUVs) were grown using the well known electroformation method [6] from mixtures of 1,2-dioleoyl-*sn*-glycero-3-phosphocholine (DOPC), and 1,2-distearoyl-*sn*-glycero-3-phosphoethanolamine-N-(biotinyl (polyethylene glycol)2000) (DSPE-PEG2000-biotin) with different ratios; all lipids were purchased from Avanti Lipids, USA. Briefly, the lipids were dissolved in a chloroform solution at an overall concentration of 2 mg ml^{-1} and then spread onto one of the walls of the electroformation cell, made of glass slides with a metallic layer of indium tin oxyde (ITO). Samples with the values 1/25, 1/50, 1/100, 1/200, and 1/500 of the relative molar concentration of DSPE-PEG2000-biotin/DOPC have been prepared. After drying the lipid film under vacuum, the cell was filled with a 100 mOsm kg^{-1} aqueous sucrose solution. A 1.5 V and 10 Hz AC voltage was applied across the 1 mm chamber gap, for circa two hours. Vesicles were then diluted in a 105 mOsm kg^{-1} TBE solution and dropped onto the DNA carpet. Osmotic pressures were measured with an Osmomat 030 Osmometer (Gonotec, Germany).

3.4 DNA carpet preparation

Double-stranded (Fermentas) λ-DNA (48502 base pairs) was end-functionalized with a molecule of biotin at each end. This was obtained by using two single-stranded oligomers (MWGBiotech), both labelled with biotin. Each oligomer is complementary to one of the protruding ends of λ-DNA and can hybridize to the corresponding overhang. After reaction, end-labelled λ-DNA was separated from the remaining free oligomers with a Nick column (Amersham). The solution of λ-DNA was diluted by adding TBE to decrease the density of DNA onto the substrate. The resulting concentration of DNA was ca. 2 ng mL^{-1}. λ-DNA was next stained with YOYO-1 (Molecular Probes), which is an intercalation fluorescent dye having a maximum adsorption at a wavelength of 491 nm and a maximum emission at 509 nm. The dye/base pair ratio was 1/5, which increases the length of λ-DNA to 22.0 μm [2] (16.5 μm without fluorescent dye [3,7]). The substrate was incubated during circa 30 minutes in the DNA solution, leading to the desired density of grafted DNA. After incubation the substrate was rinsed with a 105 mOsm kg^{-1} TBE buffer in order to remove unbound DNA.

3.5 DNA profile analysis

We have developped a homemade analysis software, to extract the main intensity line of a DNA as obtained from fluorescence imaging, with a high resolution of circa 0.25 pixel, corresponding to ≈ 0.037 μm. The method, inspired by a work published elsewhere [8], uses a weighted mean in four directions of the grey level profiles to extract individual characteristic points with sub-pixel coordinates, separated from one another by a distance of circa one pixel, the whole forming the main intensity line of the DNA. The software further gives the fluorescence intensity profile along the DNA, as the cumulated intensity along the direction transverse to the local molecule profile.

3.6 Simulation program for loop formation

We describe here a simulation procedure for the stretching and confining of a double-end grafted polymer by a spreading, adhering membrane. The simulation is valid

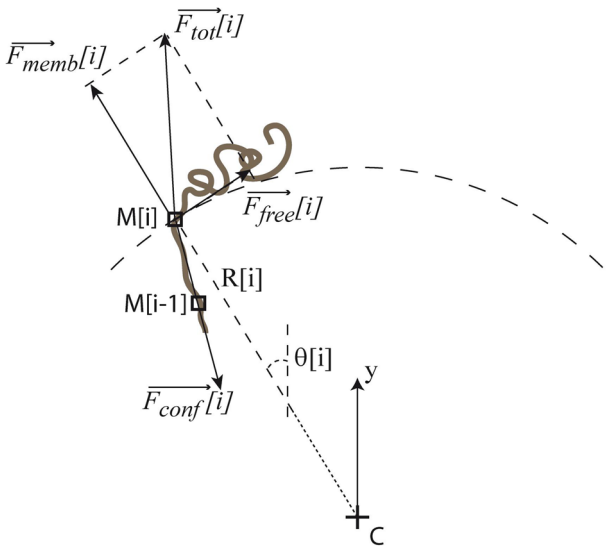

Fig. 8. The force balance at one step of the simulation program of the embedded loop formation. The dotted arc is the membrane front. M[i] is the contact point between the membrane front and the DNA on the left side of the molecule (same event is assumed to take place symmetrically with respect to the y-axis). The DNA is in a partly stretched but still free to fluctuate configuration in front of the membrane front. On the contrary, it is embedded in a tunnel backwards to the membrane front.

for stretching of both single-end grafted and double-end grafted chains. We reduce the dimensionality of the problem into a radial, 1D problem for single-end grafted DNA on one side, and into a planar, 2D problem for double-end grafted DNA on the other side. The extension of the molecule in the vertical space, above the substrate, of order of 10 nm is neglected. We rely on our previous study where we showed that two main regions can be distinguished in the very front of a spreading membrane pushing away an end-grafted molecule [1]: for high elevations above the substrate, *i.e.* above several tens of nanometers, the membrane wall can be considered as an expanding cylinder, with a velocity v of *circa* one to ten $\mu\mathrm{ms}^{-1}$, generating a radial fluid flow with a similar velocity that decreases with the distance r from the centre of the patch. In this part of the space, the stretching of the coil appears lower that a few μm. On the contrary, in the second characteristic region of the spreading, *i.e.* very close to the surface, the flow possesses a shear structure with shear rate roughly given by v/h where h is the thickness of the patch gap. For velocities in the range $\mathrm{v} = 1$ to 10 $\mu\mathrm{ms}^{-1}$ and $h \sim 10$ nm, the shear rate $\dot{\gamma}$ ranges from $\sim 10^2$ to $10^3\,\mathrm{s}^{-1}$: such shear rates are able to generate high stretching, similar to those observed in this study. Thus, the high level of stretching of the molecule is achieved exclusively in this low thickness region above the substrate; we model this stretching mechanism by considering the forces at play to be parallel to the adhesion plane.

We depict the geometry of the double-end grafted chains on Fig. 8, where focus is made at a given moment during membrane spreading, while part of the molecule is allready stretched and confined inside the membrane substrate gap, and the rest of the molecule is in a partly stretched state, confined between the bottom substrate and the membrane front. The DNA molecule lies in the plane. We impose a force balance at the contact point between the macromolecule and the membrane, *i.e.* on the monomer that is at the frontier between the embedded part of the molecule, behind the advancing membrane front, and the free part of the chain, that is pushed away by the front.

We assume at each step [i] of the simulation that the membrane front exerts a force $\mathbf{F}_{memb}$ radially oriented and of constant amplitude throughout the whole process, *i.e.* $\|\mathbf{F}_{memb}[\mathrm{i}]\| = F_{memb}$ (Fig. 8). Originating from the DNA stretching, two other forces contribute to the force balance on M[i]: on one side, the force $\mathbf{F}_{free}[\mathrm{i}]$ is exerted by the part of the DNA molecule that is in a partially stretched configuration (membrane front side), while on the other side, the force $\mathbf{F}_{conf}[\mathrm{i}]$ is exerted by the embedded part of the molecule (tunnel side) (Fig. 8). We further assume that at point $M[i]$ the force is transmitted by a pulley-like point. Therefore, the force balance on the contact point between the membrane and the DNA can be represented by the set of equations:

$$\mathbf{F}_{free} + \mathbf{F}_{memb} = \mathbf{F}_{tot} \tag{1}$$

$$\|\mathbf{F}_{tot}\| = \|\mathbf{F}_{conf}\|. \tag{2}$$

The force along the free, fluctuating, part of the DNA $\mathbf{F}_{free}$ is given by the so-called Marko-Siggia equation [9]:

$$\frac{l_p}{k_B T}\|\mathbf{F}_{free}\| = \alpha_{free} - \frac{1}{4} + \frac{1}{4(1-\alpha_{free})^2} \tag{3}$$

and at each step [i] $\alpha_{free}[i] = 2\ R[i]\theta[i]/L_{free}[i]$ is the stretching degree of the free part of the chain, of contour length $L_{free}[i]$. As sketched in Fig. 8, $R[i]$ and $\theta[i]$ correspond to the distance to the adhesion patch center of the contact monomer M[i], and to the angle of the CM[i] segment with the loop main axis, respectively.

The force along the embedded part of the DNA is given by a confined Marko-Siggia equation [10]:

$$1 - \alpha_{conf} = \frac{1}{4}\left(\frac{1}{\sqrt{\left(\frac{l_p}{w}\right)^{\frac{4}{3}} + \frac{l_P}{k_B T}\|\mathbf{F}_{conf}\|}}\right. \tag{4}$$

$$\left. + \frac{1}{\sqrt{\left(\frac{l_p}{h}\right)^{\frac{4}{3}} + \frac{l_P}{k_B T}\|\mathbf{F}_{conf}\|}}\right) \tag{5}$$

and at each step [i] $\alpha_{conf}[i] = l_{app}[i]/L_{conf}[i]$ is the stretching degree of the embedded part of the DNA, $l_{app}[i]$ is the total length of membrane tunnel, *i.e.* the sum of the left and right tunnel lengths, and $L_{conf}[i]$ is the embedded DNA contour length (sum of left and right sides). Also, the conservation equation $L_0 = L_{free}[i] + L_{conf}[i]$ has to be fulfilled at each step [i].

To simulate the whole process of loop formation, we decompose it into a set of numerical steps, during which the membrane spreads by a small distance, embedding a new fraction of DNA in the membrane-substrate gap. At step [0] the membrane advancing front reaches the two grafted ends A and B of a DNA molecule of contour length L_0. Indeed we impose for simplicity that A and B are at the same distance from the adhesion center, on both sides of the y-axis, so that at each numerical step two embedding tunnels grow symmetrically by a tunnel length δl_0, with a local orientation given by the local force balance at the contact point between the DNA and the membrane advancing front, as shown in Fig. 8 at step [i], for the left side of the molecule.

Building step [i+1] consists into adding to the existing confining tunnel previously ending at M[i], a supplemental length δl_0 oriented through the direction given by $\mathbf{F}_{tot}[\mathrm{i}]$, *i.e.* creating a new contact point M[i+1] between the membrane and the DNA, so that $\overrightarrow{M[i]M[i+1]} = \mathbf{F}_{tot}/\|\mathbf{F}_{tot}\|\delta l_0$ (symmetrically, a supplemental tunnel length is added to the other DNA strand). Then $\mathbf{F}_{conf}[\mathrm{i}]$ is first introduced in Eq. (5) so to get $\alpha_{conf}[i+1]$, the average value of the stretching degree of the embedded

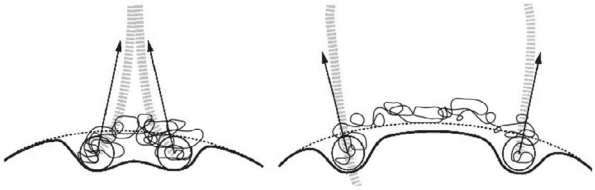

Fig. 9. Sketch of membrane deformation in the region of the membrane advancing front, when the membrane reaches a double-end grafted DNA. At each grafted end the chain exerts a force on the membrane, that creates a concave zone of a size of the order of the radius of gyration of the chain R_G [13], *i.e.* ca. 0.7 μm for λ-DNA [15]. Left: when the distance between the two grafting ends is smaller than ca. $2R_G$, the two concave zones merge, resulting in a net inward force applying to the strands, that leads to the formation of an Eiffel tower during spreading; right: above this characteristic distance, the two grafted ends are far enough so that the concave zones do not overlapp, leading to a net radial membrane force, that generates a loop during spreading.

DNA fraction over the new tunnel length $l_{app}[i+1]$. From this, we get the contour length $L_{conf}[i+1]$ and the corresponding length $L_{free}[i+1]$. Then, from the location of $M[i+1]$, the two forces $\mathbf{F}_{free}[i+1]$ and $\mathbf{F}_{conf}[i+1]$ are obtained using Eq. (3) and Eq. (5). This simulation procedure does not ensure self consistency, since the value of $\mathbf{F}_{conf}$[i] is used to calculate the DNA fraction that remains embedded at the end of step [i+1], while the stretching force at that point should be $\mathbf{F}_{conf}$[i+1]. However, increasing the number of numerical steps is expected to decrease the error of this simplified way of calculating the stretching degree of the molecule. In particular, we noticed that over one hundred steps, the structure of the final loop converges nicely through final shape and stretching state. Moreover, we also checked that as a result of this non self-consistency, the stretching degree of the confined fraction of the DNA does not evolve too much with time, during the spreading process: over all the significant situation tested, the stretching ratio of the DNA does not vary by more then two percent from the begining of the stretching process to the final step of loop formation.

The DNA persistence length is taken as $l_p = 50\,\text{nm}$ [2], and the tunnel height as $h = 10$ nm (see above). The precise determination of the tunnel width w is out of our experimental capabilities, but a good estimation of w can be obtained from the two following limiting cases: first, assuming that the biotin-streptavidin bond density in the adhesion region remains identical to the average surface density of biotins in the membrane before the adhesion takes place, one gets $w = \sqrt{s_{lip}/\rho}$, where $s_{lip} = 65$ Å^2 is the surface area occupied by a DOPC molecule [11]. Then, for ρ ranging in [1/25..1/500], w ranges in [4..18] nm, corresponding to an assumption already made in [10]. Alternatively, assuming that the DNA loop is stabilized in its confining tunnel so that the net internal force $\|\mathbf{F}_{conf}^{final}\|$ is zero, then for $\alpha_{conf} =< \alpha_{conf}^{final} >$ ranging in [0.80..0.90] (Fig. 3) Eq. (5) leads to w ranging in [16 nm..0 nm], with a non zero internal force for $\alpha_{conf} > 0.91$. Thus, the ligand densities in our vesicles are compatible with the creation of a confining tunnel of width of a few nanometers, of the order of what is necessary to get high values of the DNA stretching degree as the one measured here (Fig. 3). In our simulation program we used the value $w = \sqrt{s_{lip}/\rho}$ for the tunnel width.

4 Conclusions

The present study brings new insight on the interaction between a fluid membrane and a single macromolecule, as occuring in membrane spreading above a sparse

DNA carpet. Confinement of a single polymer by membranes or other soft walls have allready been treated theoretically and numerically for equilibrium states; see for example [12] for the case of a long polymer in a soft tube, and [13,14] for a single polymer in the gap between a membrane and a flat wall. In these cases, the equilibrium conformation of the chain results from competition between membrane bending rigidity, polymer confinement energy, and membrane adhesion in the latter case. Various types of the polymer conformation have been observed, from elongated chains to more or less swollen globular or tubular states. In the present study however, the spreading of the membrane takes places at a rate that is faster than the slower relaxation time of the chain, leading to a strong stretching of the chain during spreading that is further fixed by the rapid stappling process of the biotin ligands on the streptavidinated surface. In our previous study on single-end grafted DNAs, the geometry was mainly 1D, with a unique force at play during the membrane-DNA interaction, *i.e.* the radial membrane pushing force $\mathbf{F}_{ext}$. On the contrary, at least a 2D geometry emerges for double-end grafted DNA, with two forces competing during the membrane spreading, *i.e.* the membrane radial pushing force on one side, and the DNA internal stretching force $\mathbf{F}_{free}$ on the other side. The latter, oriented along the fluctuating and partly stretched fraction of the DNA that is pushed away by the advancing front, is always perpendicular to $\mathbf{F}_{ext}$, *i.e.* parallel to the membrane advancing front, and oriented inwards through the DNA center of mass, leading undoubtedly to a loop shape as indeed observed. Considering a simple model of force balance applied to the DNA monomer that is in contact with the membrane advancing wall, we build a step-by-step simulation process that predicts the monomer density distribution and the final shape of a double-end grafted DNA submitted to such forces. In particular our simulation method creates DNA loops with a stretching degree close to the observed ones for values of the membrane pushing force $\|\mathbf{F}_{ext}\|$ in the range 3 to 10 k_BT/l_P. However, to quantitatively reproduce the observed experimental trend, *i.e.* the existence of two initial, radially stretched ends of the DNA molecule closed by a "V"-like cap, a threshold condition on the effectiveness of the internal force has to be introduced into the above force balance, *i.e.* $\mathbf{F}_{free} = \mathbf{0}$ if $\|\mathbf{F}_{free}\| < f_{thres}$. Such effect, surprising at first sight, suggests that a non-trivial interaction between the membrane and the DNA occurs at the spreading front. An interesting possibility would be that the pressure applied by the DNA molecule on the membrane [13] creates a concave zone that laterally confines the DNA. This in turn could explain the generation of Eiffel towers, since when two of such concave depressions are very close, a net inward force could result that brings two strands together (Fig. 9).

I. Seuffert and M. Khaksar are gratefully thanked for their help with DNA functionalization. M. Basler is aknowledged for continuous experimental support. We thank Pr. Thomas Gisler and Pr. Georg Maret for fruitfull discussions.

References

1. M.-L. Hisette, P. Haddad, T. Gisler, C.M. Marques, A.P. Schroder, Soft Matter **4**, 828 (2008)
2. K. Guenther, M. Mertig, R. Seidel, Nucl. Acids Res. **38**(19), 6526 (2010)
3. P.S. Doyle, B. Ladoux, J.-L. Viovy, Phys. Rev. Lett. **84**, 4769 (2000)
4. J. Rädler, E. Sackmann, J. Phys. II (France) **3**, 727 (1993)
5. L. Limozin, K. Sengupta, Chem. Phys. Chem. **10**(16), 2752 (2009)
6. M.I. Angelova, D.S. Dimitrov, Faraday Disc. Chem. Soc. **81**, 303 (1986)
7. S.B. Smith, Y. Cui, C. Bustamante, Science **271**, 795 (1996)
8. J. Pécréaux, H.-G. Döbereiner, J. Prost, J.-F. Joanny, P. Bassereau, Eur. Phys. J. E. **13**, 277 (2004)

9. J.F. Marko, E.D. Siggia, Macromolecules **28**(26), 8759 (1995)
10. G. Nam, M.-L. Hisette, Y.L. Sun, T. Gisler, A. Johner, F. Thalmann, A.P. Schroder, C.M. Marques, N.-K. Lee, Phys. Rev. Lett. **105**(8), 088101 (2010)
11. N. Kucerka, M.-P. Nieh, J. Katsaras, Bioch. Biophys. Acta. **1808**, 2761 (2011)
12. F. Brochard-Wyart, T. Tanaka, N. Borghi, P.G. de Gennes, Langmuir **21**(9), 4144 (2005)
13. F. Thalmann, V. Billot, C.M. Marques, Phys. Rev. E **83**(6), 061922 (2011)
14. Y.-Ch. Su, J.Z.Y. Chen, Soft Matter **9**(2), 570 (2013)
15. A. Balducci, P. Mao, J. Han, P.S. Doyle, Macromolecules **39**, 6273 (2006)